A SEARCH FOR RADIO-QUIET GAMMA-RAY PULSARS

A. M. CHANDLER,[1] D. T. KOH,[1] R. C. LAMB,[1] D. J. MACOMB,[2] J. R. MATTOX,[3] T. A. PRINCE,[1] AND P. S. RAY[4]

ABSTRACT

Most Galactic point sources of gamma rays remain unidentified. The few (extrasolar) sources that have been identified are all young, rotation-powered pulsars, all but one of which were identified using radio ephemerides. The radio-quiet Geminga pulsar was identified only after pulsations were discovered in a coincident X-ray source. Observational evidence indicates that many of the unidentified Galactic sources are likely to be pulsars, and some theoretical models predict a potentially large population of radio-quiet gamma-ray pulsars. We present a new method for performing sensitive gamma-ray pulsar searches. We used this method to search several of the strongest EGRET sources for pulsations. This was a blind search for new pulsars, covering a frequency and a frequency-derivative phase space large enough to detect Crab-like pulsars as well as lower frequency, high magnetic field "magnetars." No new pulsars were discovered, and we report upper limits constraining the characteristics of any signals contained in the data sets searched.

Subject headings: gamma rays: observations — pulsars: general

1. INTRODUCTION

The nature of the unidentified Galactic plane gamma-ray sources has been a long standing problem, dating back to the first dedicated gamma-ray astronomy satellites of the 1970s (*SAS 2* and *COS B*). Despite vast technical improvements over earlier missions, the *Compton Gamma Ray Observatory* (*CGRO*) has only compounded the problem; although a small number of identifications have resulted from *CGRO* observations, many new unidentified sources have been discovered. Less than 10% of the currently cataloged Galactic plane gamma-ray sources have been identified. The principal difficulty is the large uncertainty in the gamma-ray positions. A typical gamma-ray source error box may contain hundreds of possible counterparts at other wavelengths. Nevertheless, all the identifications of persistent gamma-ray sources have been established through such multiwavelength correlations. In this paper, we describe an unsuccessful attempt to identify several of the strongest high-energy gamma-ray sources via the direct analysis of the gamma-ray data. Specifically, we attempted to identify them as pulsars.

Of the four instruments on board the *CGRO*, EGRET is sensitive to the highest energy range, about 20 MeV to 30 GeV. Details of EGRET's design and capabilities can be found in Kanbach et al. (1989) and Thompson et al. (1993). Generally speaking, it simultaneously offers good imaging (source localization to within $\sim 0°.5$), spectral resolution ($E/\Delta E \sim 5$), and temporal resolution ($\sim 50 \mu s$).

Shortly after the 1991 April launch of the *CGRO*, an EGRET all-sky survey was begun. During this first phase of its mission, EGRET verified ~ 15 previously known *COS B* sources and discovered dozens of new point gamma-ray sources (Fichtel et al. 1994). As the amount of accumulated data has increased and the gamma-ray background model has improved, several updated source catalogs have been compiled (Thompson et al. 1995, 1996). The latest EGRET catalog, based on over 4 yr of data, includes 271 sources, the majority of which are unidentified (Hartman et al. 1999). The sources can be divided into two groups—those that are in the Galactic plane and those that are not. All of the identified sources in the latter group (having Galactic latitude $|b| > 10°$) are extragalactic. The 80 sources with $|b| < 10°$ include five pulsars, one solar flare, and 74 unidentified sources. Of these, a few are probably blazars seen through the Galactic plane, and as many as five are probably spurious, leaving $\gtrsim 60$ unidentified Galactic point sources of high-energy gamma rays.

Four of the five aforementioned pulsars had been seen previously at radio wavelengths: the Crab pulsar, the Vela pulsar, PSR B1706−44, and PSR B1055−52. These EGRET sources were identified by epoch-folding the gamma-ray data with the known pulsar periods (Nolan et al. 1993; Kanbach et al. 1994; Thompson et al. 1992; Fierro et al. 1993). Additionally, pulsations from PSR B1951+32 have been seen in the EGRET data (≥ 300 MeV), although this pulsar is not detected as a statistically significant point source (Ramanamurthy et al. 1995). The remaining EGRET pulsar, Geminga, was not previously detected as a radio pulsar. Its identification came only after pulsations were discovered in a coincident *ROSAT* X-ray source (Halpern & Holt 1992) and then verified in the EGRET data (Bertsch et al. 1992). Although there have been reports of extremely weak pulsations from Geminga at low radio frequencies (~ 100 MHz; see, e.g., Malofeev & Malov 1997), Geminga can still be regarded as a "radio-quiet gamma-ray pulsar."

Efforts to identify additional EGRET sources with radio pulsars have been largely unsuccessful. Many positional coincidences exist, but few of them are expected to be real associations. The most conclusive evidence for an association would be the detection of pulsations in the gamma-

[1] Space Radiation Laboratory, California Institute of Technology, MS 220-47, Pasadena, CA 91125; amc@srl.caltech.edu, lamb@srl.caltech.edu, prince@srl.caltech.edu.
[2] Laboratory for High Energy Astrophysics, NASA Goddard Space Flight Center, Code 680, Greenbelt, MD 20771; macomb@gsfc.nasa.gov.
[3] Astronomy Department, Boston University, 725 Commonwealth Avenue, Boston, MA 02215; mattox@bu.edu.
[4] E. O. Hulburt Center for Space Research, Code 7621, Naval Research Laboratory, Washington, DC 20375; paul.ray@nrl.navy.mil.

ray data. Thompson et al. (1994), Fierro et al. (1995), and Nel et al. (1996) epoch-folded EGRET data with ephemerides of over 350 radio pulsars, with no significant detections, although marginal evidence for pulsed gamma emission has been found for PSR B0656+14, PSR B1046−58, and PSR J0218+4232 (Ramanamurthy et al. 1996; Kaspi et al. 2000; Kuiper et al. 2000). Deep radio searches of EGRET source error boxes (Nice & Sayer 1997; Lundgren, Zepka, & Cordes 1995) have resulted in only one new pulsar detection, but the pulsar proved to be unrelated to the target gamma-ray source.

Despite these failures, there are a number of reasons to believe that many of the unidentified Galactic EGRET sources are indeed young, rotation-powered pulsars. First of all, the only definitive identifications of persistent Galactic sources are all pulsars. It is reasonable to assume that even if other types of Galactic sources exist, we probably have not identified all of the detectable pulsars.

Kaaret & Cottam (1996) argued that a significant fraction of the Galactic plane sources in the second EGRET catalog were located in OB associations, which are likely to house young pulsars. Using the known distances of the OB associations, they estimated the luminosities of the coincident gamma-ray sources and found them to be consistent with the known EGRET pulsars. They ultimately estimated that ~ 20 of the 25 sources in the second EGRET catalog with $|b| < 5°$ are pulsars. That these pulsars have not been detected in radio wavelengths can be attributed to the narrow beaming of radio pulses and the high interstellar dispersion expected in star-forming regions.

Sturner & Dermer (1995) found a significant correlation between the high-confidence point sources in the first EGRET catalog and supernova remnants (SNRs). SNR associations have been suggested for as many as seven of the 32 low-latitude unidentified sources in the second EGRET catalog (Sturner, Dermer, & Mattox 1996; Esposito et al. 1996). It is plausible to assert that the gamma rays are due to either a young pulsar, born in the supernova explosion, or cosmic rays accelerated in the expanding supernova shock wave. At present, neither cause can be ruled out. Several authors have argued for the presence of pulsars in a few specific cases (Bhattacharya et al. 1997; Brazier et al. 1998, 1996; Roberts & Romani 1998), but evidence for shock-front cosmic ray production also exists for several of the SNR associations. Until future missions resolve the spatial structure in the gamma-ray sources or improve their spectral characterization, conclusive identifications of shock-powered SNRs will be very difficult to establish. On the other hand, the detection of pulsations in the EGRET data has the potential to resolve the issue on a source by source basis.

McLaughlin et al. (1996) characterized the time variability of the sources in the second EGRET catalog (using data from phases 1, 2, and 3). In their classification scheme, the known EGRET pulsars were shown to be nonvariable or marginally variable. Although they argue for the existence of a genuine population of variable low-latitude sources, they also find a significant number of nonvariable low-latitude sources, which they conclude are most likely pulsars. The gamma-ray pulsar population model of McLaughlin & Cordes (2000) predicts that EGRET should see 20 (low-latitude) pulsars, a result that is consistent with the variability arguments since 17 of the unidentified low-latitude sources are nonvariable. Wallace et al. (2000)

revisited the question of EGRET source variability. Looking at shorter timescales (approximately days), they found strong evidence of short-term variability for only four unidentified cataloged sources. This result is consistent with the hypothesis that many of the unidentified sources could be pulsars.

Thus, despite indications that many of the unidentified EGRET sources are pulsars, previous attempts to identify them with radio pulsars have failed. This raises the possibility that many of the unidentified sources could be radio-quiet pulsars like Geminga. Romani & Yadigaroglu (1995) have proposed an outer gap model of pulsar gamma-ray production that predicts that pulsed gamma radiation is beamed into a larger solid angle than the radio emission. This model is shown to account for observed properties of individual pulsars (e.g., pulse profiles and the relative phase of radio and gamma-ray pulses) and the overall observed population of radio-only and radio/gamma-ray pulsars. Their model predicts a large number of detectable radio-quiet gamma-ray pulsars, 2.5 times the number of detected radio-loud gamma-ray pulsars. In a more recent analysis (Yadigaroglu & Romani 1997), they showed that radio-quiet pulsars can account for essentially all of the strongest unidentified low-latitude EGRET sources.

Another possible mechanism for producing radio-quiet gamma-ray pulses has recently been suggested. Even before the identifications of the soft gamma repeaters SGR 1806−20 and SGR 1900+14 as magnetars (Kouveliotou et al. 1998, 1999; Thompson & Duncan 1995, 1996), Baring & Harding (1997) proposed the existence of a class of high magnetic field, radio-quiet, high-energy pulsars. According to the model, intense magnetic fields can inhibit pair production, suppressing a pulsar's radio emission. A highly magnetized pulsar "can still emit gamma rays prolifically." While there has been a report of weak, low-frequency radio pulsations from SGR 1900+14 (Shitov 1999), this is not inconsistent with the model (Baring & Harding 1998).

The EGRET instrument long outlived its intended 2–4 yr lifetime. After a gyroscope failure in 1999 December, NASA decided to deorbit the *CGRO* in 2000 June. The next-generation high-energy gamma-ray satellite, the *Gamma-Ray Large Area Space Telescope* (*GLAST*), will launch no sooner than 2005. Thus, no new pertinent gamma-ray data are expected in the near future. Searches of EGRET error boxes at other wavelengths continue, but it now seems that further application of conventional approaches is unlikely to result in new identifications. In this paper we test the hypothesis that many of the unidentified EGRET sources are radio-quiet pulsars by searching for pulsations in the existing gamma-ray data directly (Mattox et al. 1996). Previous attempts to find pulsations have involved epoch-folding with known signal parameters. We instead performed a blind search for unknown pulsars on several of the strongest EGRET point sources.

As we will explain in more detail below, this is a difficult problem. The size and number of fast Fourier transforms (FFTs) that must be calculated make this a computationally intensive problem—one that would have been infeasible 10 yr ago. Because of the small photon flux of the sources, signal-to-noise ratios (S/Ns) are very low. Special techniques must be employed to keep detection sensitivity as high as possible. Even then, we require a somewhat fortuitous pulse waveform. Despite the difficulties, even one detection would add significantly to our knowledge of

gamma-ray pulsars and pulsar emission mechanisms. Unfortunately, no candidate signal survived all of our detection criteria.

In § 2 we describe our analysis method. We indicate the specific EGRET sources we searched for pulsations and the range of pulsar frequencies and frequency derivatives to which the search was sensitive. In § 3 we describe the results of our pulsation search. We discuss the determination of detection significance and the connection between the signal waveform and detectability, which we then use to place limits on the characteristics of any signals contained in the EGRET data searched. Finally, in § 4 we discuss these results and their implications.

2. ANALYSIS

2.1. Principles

Finding a pulsar signal in the EGRET data is not a trivial problem. Even the strongest unidentified EGRET sources have count rates (≥ 100 MeV) of ~ 1 source photon hr^{-1} over a typical background of ~ 5 photons hr^{-1} (in the Galactic plane). To achieve an adequate S/N to allow an FFT search, long data sets—on the order of weeks—are required. The data sets used in the present analysis spanned 14–38 days each. The independent frequency spacing of the FFT is given by $1/T$, where T is the total duration of the time series data. The long EGRET data sets therefore result in submicrohertz spectral resolution, requiring large FFTs to cover a given frequency range.

Pulsar rotation frequencies are generally observed to decrease slowly over time. This is attributed to the conversion of rotational kinetic energy into the radiation emitted by the pulsar, hence the term "rotation-powered pulsar." Such intrinsic spin-down is not usually a problem for pulsar searches at radio and X-ray wavelengths, for which shorter data sets (approximately minutes to hours) are often used. Over a 14 day observation, however, a pulsar's spin frequency can change by as much as several hundred microhertz. The signal from such a pulsar will be spread out over hundreds of frequency bins in the FFT, rendering it undetectable.

Figure 1 shows a plot of the 472 pulsars in the Princeton catalog (Taylor, Manchester, & Lyne 1993) that are observed to be spinning down. The pulsars are plotted in a phase space of spin frequency f and its first-order time derivative $\dot{f}$. If we Taylor-expand a pulsar's frequency evolution $f(t)$, we see that over the course of an observation of duration T, the pulsar frequency will visit the range $\Delta f = \dot{f}T + \ddot{f}T^2/2 + \cdots$ (a dot denotes a derivative with respect to time, in this case, evaluated at the beginning of the observation). In the discrete Fourier spectrum, this is equivalent to a drift of $\Delta B = T \Delta f = \dot{f}T^2 + \ddot{f}T^3/2 + \cdots$ independent frequency bins. Using $T = 14$ days, we find that a frequency derivative of $|\dot{f}| = 1/T^2 = 6.8 \times 10^{-13}$ Hz s^{-1} causes a drift equivalent to one power spectrum bin. As is evident in Figure 1, many pulsars are observed with larger first-order frequency derivatives than this. Likewise, a second derivative of $|\ddot{f}| = 2/T^3 = 1.1 \times 10^{-18}$ Hz s^{-2} will cause a similar 1 bin drift. Fortunately, this is more than 2 orders of magnitude larger than the observed second-frequency derivatives. We are therefore justified in adopting a linear model for the frequency evolution.

To counteract this spin-down effect, we attempt to remove the frequency drift of a pulsar signal in the time
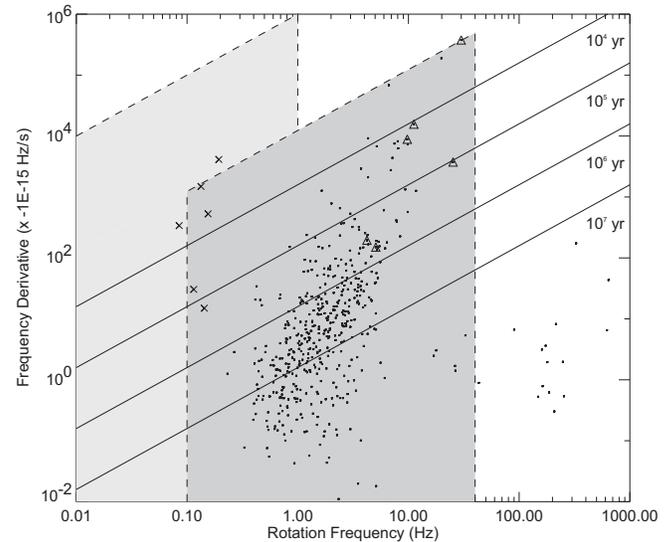

FIG. 1.—The f-$\dot{f}$ phase space relevant to our search. The 472 pulsars in the Princeton catalog (Taylor et al. 1993) that have positive period derivatives are denoted by filled circles. The known EGRET pulsars are indicated by triangles. They are, in order of decreasing rotation frequency, Crab, PSR 1951+32, Vela, PSR 1706−44, Geminga, and PSR 1055−52. The crosses denote, in order of decreasing $|\dot{f}|$, SGR 1900+14, SGR 1806−20, 1E 1048−5937, 1E 1841−045, 4U 0142+615, and 1E 2259+586. The solid lines plotted on the figure are lines of constant age for pulsars born at short periods, assuming a vacuum dipole braking law. The dark shaded region corresponds to the Crab-like pulsar search and the lighter region denotes the magnetar search phase space described in the text.

domain before calculating the FFT. In a blind search, little is known a priori about a pulsar's frequency evolution (except that its behavior is expected to be similar to that of the known pulsars). A number of frequency drift trials must therefore be performed for each source, whereby the data are corrected for an assumed frequency derivative, and an associated FFT is calculated and analyzed.

The known EGRET pulsars are highlighted (*triangles*) in Figure 1. The gamma-ray pulsars tend to have high frequencies and large (negative) values of $\dot{f}$. This is not surprising since we expect pulsars in this region of the phase space to be the most energetic, i.e., to have the largest rotational energy loss $\dot{E} = 4\pi^2 I f \dot{f}$, where I is the pulsar's moment of inertia. This fact is rather unfortunate for our purposes since the phase space that our search must cover is therefore large. For this project, we chose to cover frequencies up to 40 Hz and frequency derivatives large enough to include the Crab pulsar. This search phase space is represented by the darker shaded region in the figure. As described below (§ 2.2.2), our frequency drift search was carried out over trial values of $\dot{f}/f$, not simply $\dot{f}$. The $\dot{f}$ limit of the dark shaded region in the figure corresponds to

$$-\frac{\dot{f}}{f} \leq \frac{3.7 \times 10^{-10} \text{ Hz s}^{-1}}{30 \text{ Hz}} \approx 1.2 \times 10^{-11} \text{ s}^{-1} . \quad (1)$$

For the actual FFT calculation, we require a Nyquist frequency of $f_{\text{Nyq}} \geq 160$ Hz so that we may calculate sums of up to four harmonics without aliasing. Given the required length of the data sets, this means that we must calculate FFTs of $N = (2 \times 160)T = 2^{29}$–$2^{30} \sim 10^9$ points. Each

source requires $\sim 3.7 \times 10^{-10} T^2 \sim 10^3$ frequency-derivative trials. Such a search has only recently become computationally feasible.

2.2. Search Methodology

We began by selecting a number of unidentified EGRET sources for analysis. For each source, we prepared a data set, which is essentially a list of photon arrival times. Before beginning the search, we determined a list of frequency-derivative trials to cover our target phase space.

For a given frequency-derivative trial, the photon arrival times were corrected for the assumed pulsar spin-down rate. Using these adjusted arrival times, we calculated an FFT, which we used to construct a normalized power spectral estimate. This power spectrum was then searched for significant candidates, i.e., frequency bins containing statistically significant excess power. Sums of two and four harmonics were also searched in this way. This process was repeated for each frequency-derivative trial.

Candidates from the FFT stage of the analysis were subjected to further scrutiny. In the vicinity of each candidate, we sampled the f-$\dot{f}$ phase space more finely, again looking for significant powers. If any candidates survived this (more stringent) cut, we put them though several final verification procedures. Each of these steps is described in detail below.

2.2.1. Source Choice and Data Preparation

The unidentified EGRET sources chosen for analysis in this project were selected simply on the basis of strength. The most appropriate measure of the source strength in this case is the quantity N_s^2/N_t, where N_s is the number of source photons and N_t is the total number of photons in a data set (i.e., source plus background). This is the square of the S/N for a data set. As we show in detail in § 3, the expected spectral power from a periodic source is proportional to N_s^2/N_t, and the significance of a detection is exponential in N_s^2/N_t. So the general idea was to choose an EGRET viewing period (VP) and select a set of photon events so as to maximize N_s^2/N_t. In some cases, adjacent (or nearly adjacent) observations were concatenated. The sources so chosen and the VPs analyzed are listed in Table 1 and ranked in order of N_s^2/N_t. Also indicated in the table are possible SNR associations and the source positions, although these were not source selection criteria.

Having chosen an EGRET VP, we selected photons based on three criteria—one spectral and two spatial. Because of the diffuse gamma-ray background, the source S/N is very low for photon energies below 100 MeV. Our analysis included only photons above this threshold. The imaging capabilities of the EGRET instrument were characterized during its prelaunch calibration (Thompson et al. 1993). From the measured point-spread function (PSF), it was determined that approximately 67% of the photons from a source will be observed to come from within a cone of energy-dependent half-angle

$$\theta_{67} = 5°85\left(\frac{E_\gamma}{100 \text{ MeV}}\right)^{-0.534} \quad (2)$$

(E_γ is the photon energy). In-flight analyses of EGRET's angular dispersion characteristics have been shown to be in very good agreement with the prelaunch PSF (Esposito et al. 1999). Only photons measured to have arrived from within θ_{67} of the assumed source direction were included for analysis. Tests with the known EGRET pulsars indi-

cated that this cut was robust and optimal—small changes in this cutoff angle had little effect, and large changes either way reduced the recovered spectral power. Finally, we selected only photons that were more than 4 times this angle from the Earth limb.

The next step in the data preparation was to correct the spacecraft photon arrival times to solar system barycentric arrival times using the known position and orientation of the instrument and the assumed direction of the source. For the source directions, we used the maximum likelihood positions from the first or second EGRET catalog. The only exception is 2EG J2020+4026, for which we used the position of a coincident *ROSAT* source (Brazier et al. 1996). The actual positions used for each source are listed in Table 1. The errors on the position estimates (semimajor axis of 95% confidence error ellipse) are typically $\lesssim 0°5$ (see Thompson et al. 1995).

Our analysis was carried out before the publication of the third EGRET source catalog (Hartman et al. 1999). The updated positions in the new catalog adversely affect only two of our sources. The highly significant second EGRET catalog source 2EG J2019+3719 was split into two lower confidence detections in the third catalog (3EG J2016+3657 and 3EG J2021+3716). Although there is a significant overlap between our searched error box and the error boxes of the two new sources, neither would individually be strong enough to produce pulsations detectable in our blind search. A similar situation exists for 2EG J1021−5835 (split into 3EG J1013−5915, 3EG J1014−5705, and 3EG J1027−5817). If the third catalog is correct, we could not have detected pulsations from these weaker individual sources. We still report our search results for 2EG J2019+3719 and 2EG J1021−5835 in Tables 1 and 3, although the upper limits apply only if the second catalog is assumed to be correct.

We now consider the effect of the position uncertainties on our search. A position error of ϵ, measured in radians, leads to a Doppler shift from the Earth's orbital motion of

$$\delta f = \frac{v_\oplus}{c} \epsilon f \sin\theta = 10^{-5} \frac{\epsilon}{10^{-2}} \frac{f}{10 \text{ Hz}} \sin\theta \text{ Hz}, \quad (3)$$

where $v_\oplus/c = 10^{-4}$ is the magnitude of the Earth's orbital velocity in units of the speed of light and θ is the angle between the Earth's orbital velocity and the EGRET source direction. A pure shift of frequency will have no effect on the *detection* of pulsations, although the frequency estimate will be incorrect. In the event of a detection, the correct rest frequency of the pulsar and its position can hopefully be refined using other EGRET observations.

Differentiation of equation (3) leads to

$$\delta\dot{f} = \frac{v_\oplus}{c} \epsilon\dot{\theta}f \cos\theta + \mathcal{O}(\dot{\theta}^2), \quad (4)$$

where $\dot{\theta} = 2 \times 10^{-7}$ rad^{-1} is the Earth's orbital angular velocity. Thus,

$$\delta\dot{f} = 2 \times 10^{-12} \frac{\epsilon}{10^{-2}} \frac{f}{10 \text{ Hz}} \cos\theta \text{ Hz s}^{-1}. \quad (5)$$

This is much less than the limiting $\dot{f}$ of our search. Therefore, as for frequency, $\delta\dot{f}$ does not compromise the detection sensitivity but does prevent a precise determination of the intrinsic pulsar $\dot{f}$ unless more observations are used to esti-

TABLE 1

EGRET POINT SOURCES SEARCHED

Source	SNR	l (deg)	b (deg)	EGRET VP Analyzed	Duration (days)	N_s^2/N_t	$(N_s^2/N_t)_{eff}$	f Trials	$\alpha\mathcal{F}^2$	Pulse FWHM[a] (%)	Pulsed Fraction[b] (%)
2EG J2020+4026 …	γ Cygni	78.1	2.3	203	21	76	73	1210	<0.94	>23	<49
2EG J0618+2234 …	IC 443	189.2	3.0	0.2 + 0.3 + 0.4 + 0.5 + 1.0	38	46	32	3947	<2.14	>12	<75
2EG J2019+3719[c] …		75.46	0.60	203	18	34	27	859	<2.53	>10	<81
2EG J1835+5919 …		88.8	25.1	212	14	28	28	540	<2.44	>10	<80
2EG J1021−5835[c] …		284.45	−1.20	14	14	27	27	524	<2.53	>10	<81

[a] FWHM of a single Gaussian peak, expressed as a percentage of the pulse period; assumes 100% pulsed fraction.
[b] For typical radio pulsar waveform (see text).
[c] The third EGRET catalog (Hartman et al. 1999) split 2EG J2019+3719 and 2EG J1021−5835 into multiple sources. The upper limits reported assume the validity of the second EGRET catalog (Thompson et al. 1995; see § 2.2.1).

mate the pulsar position and rotation parameters simultaneously.

Differentiation of equation (4) leads to

$$\delta\ddot{f} = \dot{\theta}^2 \delta f + \mathcal{O}(\dot{\theta}^3) , \tag{6}$$

$$\delta\ddot{f} = 4 \times 10^{-19} \frac{\epsilon}{10^{-2}} \frac{f}{10 \text{ Hz}} \sin\theta \text{ Hz s}^{-2} . \tag{7}$$

Previously, we noted that an $\ddot{f}$ of approximately $2/T^3 \sim 10^{-18}$ Hz s^{-2} would require a search over trial $\ddot{f}$ values like the $\dot{f}$ search. For our search phase space, including frequencies up to 40 Hz, we see that $\delta\ddot{f}$ is of this same order. Since we did not include frequency second-derivative trials in our search, we must carefully consider the effect $\delta\ddot{f}$ has on our search sensitivity.

The effect of the position error is to cause a source frequency to drift over time. In the FFT, the signal power will be spread over several spectral bins. If we require that this spreading not exceed some fixed number of bins over the course of an entire observation, we see from equation (7) that we can cover the full source error box in a restricted frequency range or cover the full 40 Hz frequency range over a smaller region of the error box. Alternatively, we can claim sensitivity to the entire error box over the entire range of search frequencies by reducing the effective source strength. After we correct for $\dot{f}$, the apparent source frequency diverges from its initial value according to $\Delta f(t) = \delta\ddot{f}t^2/2$. Equivalently, in units of independent Fourier bins, $\Delta b(t) = \delta\ddot{f}Tt^2/2$. The fundamental has drifted over a range equivalent to one spectral bin after a time $t_1 = [2/(\delta\ddot{f}T)]^{1/2}$. Since the source strength parameter N_s^2/N_t scales linearly with time, only a reduced effective signal strength of

$$\left(\frac{N_s^2}{N_t}\right)_{\text{eff}} = \frac{t_1}{T} \frac{N_s^2}{N_t} = \left(\frac{2}{\delta\ddot{f}T^3}\right)^{1/2} \frac{N_s^2}{N_t} \tag{8}$$

has been confined to an acceptable range. The effective strength $[N_s^2/N_t]_{\text{eff}}$ for each source is listed in Table 1. These values were used to determine the sensitivity limits of our search. Note that not all of our target sources were affected by position error, and for those that were, the sensitivity is actually nonuniform over the source error box and searched frequency range. The limits reported are for the worst case scenario: $f = 40$ Hz and extreme position error (source located on its 95% error contour).

2.2.2. Frequency-Derivative Trials

Ultimately, a data set consisted of a list of each photon's barycentric time of arrival (TOA). We assume that the data contain a signal whose frequency evolves in time according to $f(t) = f_0 + \dot{f}t$. In order to remove the frequency drift, we introduce a new time $\tilde{t}$, which is a function of the original time t such that the frequency as a function of $\tilde{t}$ is constant. Equivalently, we require the integrated phase to be linear in $\tilde{t}$:

$$\phi(t) - \phi_0 = \int_0^t f(t')dt' = f_0\tilde{t} . \tag{9}$$

The ith TOA t_i (measured from $t_0 = 0$) will therefore be corrected to

$$\tilde{t}_i = t_i + \frac{1}{2}\frac{\dot{f}}{f_0}t_i^2 . \tag{10}$$

A time series is constructed by dividing the total duration of the data T into N bins. The entire array is initially set to zero, then for each TOA, the value in the corresponding time bin is increased by 1. Before being corrected, the ith TOA would fall into bin $b_i = t_i/\Delta t$, where $\Delta t = T/N$, which is the resolution of the time series. We can then express the frequency-derivative correction in terms of bin number

$$\tilde{b}_i = b_i - \frac{b_i^2}{a^2} , \tag{11}$$

where the parameter a is given by

$$a = \sqrt{\frac{2f_0}{\Delta t |\dot{f}|}} \tag{12}$$

(note that $\dot{f} < 0$).

The spacing of the $\dot{f}$ trials is chosen so that the fourth harmonic of a Crab-like pulsar will drift by no more than two power spectrum bins over the course of the entire observation. This results in a maximum trial spacing of $\Delta\dot{f}_{\text{trial}} = 1/T^2$. We use a fiducial $f_0 = 30$ Hz in equation (12) and search up to $\dot{f}_0 = -3.7 \times 10^{-10}$ Hz s^{-1}. The number of $\dot{f}$ trials required for a given source is then

$$N_{\dot{f}} = \frac{|\dot{f}_0|}{\Delta\dot{f}_{\text{trial}}} = 3.7 \times 10^{-10}T^2 . \tag{13}$$

The resulting numbers are listed in Table 1.

2.2.3. FFT and Initial Candidates

Having prepared a TOA list and generated a list of trial frequency derivatives for a given source, we proceeded with the first stage of the actual search. For each $\dot{f}$ trial, we constructed a time series as per § 2.2.2. We used this time series to calculate an FFT, from which we calculated the power spectrum. We then searched this power spectrum for significant peaks (single harmonics and harmonic sums). As a whole, this step was the most computationally intensive part of the analysis, involving the calculation of almost 10^4 billion-point FFTs, including all the sources searched. The gigapoint FFTs were calculated in-core using the 512 processor Intel Touchstone Delta supercomputer.

If a single power spectrum bin contained power that exceeded a predetermined threshold, then the corresponding f and $\dot{f}$ values were saved for further analysis. The FFT is most sensitive to source frequencies that are exactly equal to the discrete Fourier frequencies (integer multiples of $1/T$). When the source frequency is not equal to a Fourier frequency, the signal power can be spread over several power spectrum bins, and the single bin peak power can be reduced by almost 60%. Even in this worst case, however, 80% of the power will still be in the two bins closest to the source frequency. For this reason, and also to allow for some frequency drift due to $\dot{f}$ error, we also saved candidates that showed significant power in a sum over neighboring spectral bins. Since gamma-ray and radio pulsar signals tend to have a rich harmonic content, we computed two- and four-harmonic power sums, again saving the best candidates. Neighboring bins were also included in the harmonic sums.

The end result of this stage of the search was a list of $(f, \dot{f})$ candidates corresponding to the top one-, two-, and four-harmonic powers. The minimum power thresholds were set very low, resulting in $\sim 10^3$ candidates of each type

from each source. Obviously, virtually all of these candidates are expected to be due to random noise fluctuations.

2.2.4. *Post-FFT Analysis*

Because of the small number of photons in a data set ($N_t \sim 10^3$), small sections of power spectra can be calculated with minimal computational effort. The raw (unnormalized) power in bin k is given by

$$P_k^{\text{raw}} = \left| \sum_{j=0}^{N-1} x_j e^{-2\pi i jk/N} \right|^2, \tag{14}$$

where x is the spin-down–corrected time series described above and $N = 2^{30}$ is the total number of points in the time series. Since only N_t of the N time series points are nonzero, we can reduce the sum over N to a sum over N_t. If we globally normalize the power spectrum to a mean value of 1, equation (14) becomes

$$P_k = \frac{1}{N_t - N_t^2/N} \left| \sum_{j=0}^{N_t-1} e^{-2\pi i \tilde{b}_j k/N} \right|^2, \tag{15}$$

where $\tilde{b}_j$ is the corrected bin number of the jth photon. This requires only $\sim N_t \sim 10^3$ floating point calculations per frequency bin (and very little memory). It is therefore a simple matter to calculate sections of power spectra in the vicinity of the FFT candidates on a workstation computer. We take advantage of this fact to refine our candidate list.

In the neighborhood of each candidate, we searched a local f-$\dot{f}$ phase space with higher resolution. Compared with the FFT search, we reduce the spacing of the $\dot{f}$ trials by a factor of 8, and by oversampling the power spectrum, we reduce the spacing of the frequency trials by the same factor. The result is a significant decrease in the spin-down–induced frequency drift and the power loss due to the discrete Fourier sampling, obviating the neighboring bin sums. For a real signal, roughly the same signal power is recovered but in fewer power spectrum bins, dramatically increasing the detection significance. An example illustrating the effectiveness of this method is given in § 2.4.

2.2.5. *Final Verification Procedures*

At this stage, we attempted to confirm or refute the strongest candidate detections by means of several final tests. One such test was to look for spectral power in higher harmonics. Since the search only included sums of up to four harmonics, this method was used primarily to check for power in the fifth through eighth harmonics of four-harmonic candidates. Note that this is a statistically independent test. Since the candidates resulted from a search involving many trials (over 10^{12} four-harmonic sums were calculated in the FFT stage of the analysis), a large four-harmonic power was required for a candidate to survive the search stage. Checking the next four harmonics involves only one trial for each of the final candidates (of which there were $\sim 10^2$), so a little excess power can be highly significant. Of course, candidates were not rejected simply on the basis of this test since the typically broad, multicomponent waveforms of gamma-ray pulsars may not exhibit significant power in the higher harmonics.

For each candidate, we also folded a pulse profile. This is essentially a histogram of photon counts as a function of the pulse phase. The pulse phase of a photon is equal to its arrival time modulo the putative pulse period. Pulse profiles (also known as light curves) can be usefully analyzed "by eye" for comparison with known pulsars or possible emission models. They can also be used to calculate a statistical significance by determining the probability that a given profile could have resulted from a flat distribution.

Another powerful verification technique involved photon weighting. In the initial search, photons were selected from an EGRET observation, as described in § 2.2.1. All photons that made the cut in equation (2) were given equal weight in the construction of the time series and the calculation of the power spectrum. In reality, the EGRET PSF is not shaped like a step; the larger a photon's angular separation from a source, the less likely it is to have originated from that source. Using the derived EGRET (source-free) background model and the measured PSF, we applied weights to the photons in a data set and recalculated a candidate's spectral power. Testing this method on real and simulated EGRET pulsars showed that signal power could be increased by 15%–70%. The smaller gains came from using the exact same photons as were originally used. The larger gains came from using more photons—either extending the angular cutoff out to where the PSF is essentially zero or extending it to lower energies (<100 MeV) or both. At the power levels of our candidates, even a 20% gain can increase a candidate's significance by several orders of magnitude.

The above confirmation procedures can be extremely useful in weeding out noise fluctuations and increasing the confidence of real signals, but perhaps the most conclusive verification of a candidate would be to detect the same pulsation in a different observation of the same source. In practice, this can be very difficult. The measured frequency and frequency derivatives are subject to small but nontrivial errors. When we also take the position uncertainty into account and propagate forward or backward to the second observation, the f-$\dot{f}$ phase space we must search is considerable. Of course, this phase space is small compared to the original search space, but it is not insignificant. If the two observations have comparable source count rates and are not widely separated in time, then verification may be possible. But even a slight reduction in source strength and a separation of several months can make the source signal impossible to distinguish from noise in the second observation.

2.3. *Magnetar Search*

In addition to the search for Crab-like pulsars that we have been describing so far, we also ran a separate search over a phase space more suited to detecting magnetars. Although they are not in the Princeton catalog, we have indicated six known or suspected magnetars in Figure 1. The soft gamma repeaters SGR 1806−20 and SGR 1900+14 and the anomalous X-ray pulsars 1E 1841−045, 1E 1048−5937, 4U 0142+615, and 1E 2259+586 are marked with crosses in the plot (Baring & Harding 1998 and references therein). (Note, however, that in some cases, the $\dot{f}$ errors are larger than the plotted symbols). They are clearly distinguished from the "normal" pulsars by their low rotation frequencies and comparatively large spin-down rates. This combination implies a large surface magnetic dipole field and gives the magnetars their name. For this search, we chose to cover the lighter shaded region in Figure 1: frequencies from 0.01 to 1.0 Hz and $-\dot{f}/f < 1 \times 10^{-9}$ s^{-1}. This region includes magnetic fields up to approximately 2×10^{15} G at $f = 1$ Hz and 2×10^{17} G at $f = 0.01$ Hz. The search was technically very similar to

the Crab-like search, with several exceptions that we now describe.

There are indications that the long-term frequency evolution of magnetars may not be well described by a simple low-order expansion, i.e., by the lowest order frequency derivatives (Kouveliotou et al. 1999; Melatos 1999). For this reason, we chose to shorten our two longest data sets, as compared to the Crab-like search, and to include $\ddot{f}$ trials in our frequency drift corrections (up to $|\ddot{f}| < 3 \times 10^{-18}$ Hz s^{-2}, both positive and negative values). Since the frequency range we wanted to cover was smaller, the FFTs could be smaller, but the number of required spin-down corrections was much higher. Treating each order derivative separately, we decided to limit the effect of each so that the fourth harmonic of any signal in the search phase space would drift by no more than the equivalent of one power spectrum bin. This necessitated a trial $\dot{f}$ spacing of $\Delta \dot{f}_{\mathrm{trial}} = 1/2T^2$ and a trial $\ddot{f}$ spacing of $\Delta \ddot{f}_{\mathrm{trial}} = 1/T^3$. For a 14 day data set, this amounts to over 3×10^4 spin-down trials (per source).

To reduce this number, we decided to utilize incoherently stacked power spectra (see, e.g. Brady & Creighton 2000). The continuous data set is divided into a number of smaller sections, and a power spectrum is calculated for each. The separate spectra are then added together. If we divide the data into $\mathscr{S}$ sections, the independent Fourier spacing is increased by a factor of $\mathscr{S}$. We can therefore tolerate more frequency drift, and the total number of drift trials goes down by a factor of $\mathscr{S}^2$ (one factor of $\mathscr{S}$ for each of the two search parameters $\dot{f}$ and $\ddot{f}$). For this search, using $\mathscr{S} = 4$ stacks for all sources brought the number of trials down to an acceptable value, with only about a 20% reduction in sensitivity as compared with the coherent (single stack) method.

We calculated the power spectra with an oversampling factor of 2. Neighboring bin sums were not used for the two- and four-harmonic candidates. The single harmonic candidates included significant single bin powers and neighboring bin sums. These sums were, of course, of *independent* bins and not truly neighboring bins, which are not independent in an oversampled spectrum. Good candidates were put through the same kinds of final analyses as described above for the Crab-like search. Note that the $\ddot{f}$ search absorbs the effect of the position error, so we need not consider reduced source strengths when calculating the sensitivity of the magnetar search.

2.4. *Testing Our Method on Geminga*

Our method easily detects the known strong EGRET pulsars (Crab, Vela, and Geminga). The FFT stage alone detects each of them with better than $S \sim 10^{-50}$ significance (S is essentially the probability that the observed spectral power was produced by random noise fluctuations). Figure 2 shows a section of the Geminga power spectrum calculated from VP 1.0 data prepared as described above. Only spectral bins with power $P > 7$ are plotted. The three highest peaks correspond to the first, second, and fourth harmonics of Geminga's 4.2176751 Hz rotation frequency. Most of the power is in the second harmonic. This is understandable since Geminga's pulse profile, shown below in the figure, has two peaks separated by about 180° in phase.

We can simulate a weaker source by selecting a subset of the data. If we include only every nth photon, the source strength N_s^2/N_t scales down by a factor of $1/n$. We now
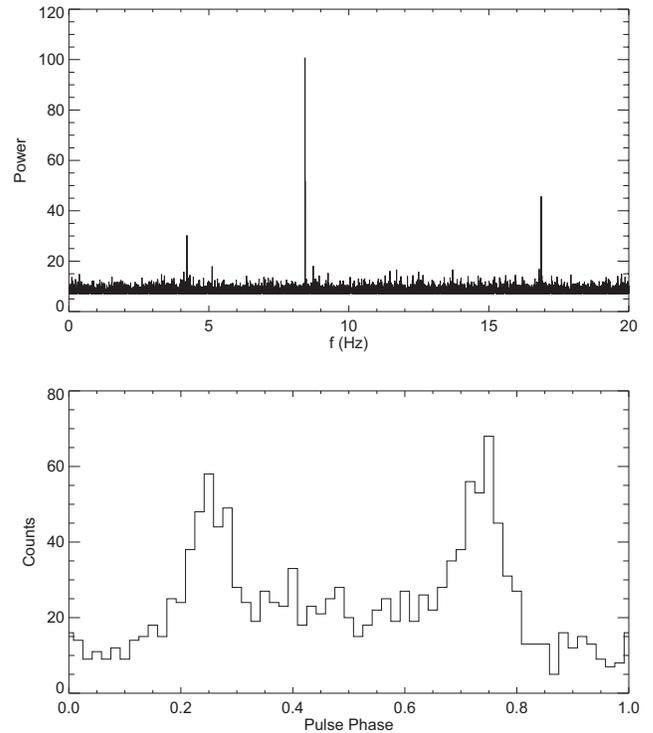

FIG. 2.—Section of the power spectrum from the EGRET VP 1.0 observation of Geminga along with the corresponding pulse profile

illustrate the main steps of our search method using a data set consisting of every sixth VP 1.0 Geminga photon. The data set contained 232 photons, 126 of which are expected to have actually come from Geminga, yielding $N_s^2/N_t = 68$. This is comparable to our strongest unidentified source.

The pulsar shows up in the FFT candidate list with a four-harmonic power of 47.51. Note that this is a sum of power from 12 spectral bins, three consecutive bins at each of the four harmonics. We did not run an entire set of frequency-derivative trials; Geminga's small $\dot{f}$ is actually covered by the first $\dot{f}$ trial. Even so, it was not the highest candidate in the list. Had we run all 540 trials, we would have expected to see about 20 noise candidates with at least this much power. Still, this power was well above the threshold we used in the actual searches (our four-harmonic [12 bin] power cutoff was 44, which should produce $\sim 10^3$ noise candidates per source). So at this stage, the pulsar signal has made our candidate list but is certainly not significant.

When we refine the search space in the vicinity of the FFT candidates, the pulsar signal emerges above the noise. After the local oversampling analysis, the weakened Geminga has a four-harmonic, 4 bin power of 40.88. This was by far the best candidate remaining. If we consider only the full Geminga search, the candidate now has a significance of $S \sim 0.09$. If we take all the searches into account, the significance is only $S \sim 0.9$, but this is well within the range of candidates that were subjected to the final verification procedures. In fact, this would have been our second best search candidate at this point.

Although the power in the next four harmonics is not significant, the profile alone looks good enough to warrant attempting a search in other observations. But we can convincingly verify the detection in this data set by PSF-

TABLE 2
TEST RESULTS FOR WEAKENED GEMINGA DATA (see text)

Parameter	After FFT	After Local Analysis	After PSF Weighting
Four-harmonic Power	47.51	40.88	55.56
Spectral Bins Summed......	12	4	4
Significance	~ 1.0	~ 0.9	$\sim 10^{-6}$

weighting the photons. With the weighted data, the four-harmonic spectral power increases to 55.56, with significance $S \sim 10^{-6}$, taking all the search trials into account. The main steps of this analysis are summarized in Table 2.

3. RESULTS

No candidate from any source passed all of our detection criteria. In § 3.1, we describe the statistics used to determine the significance of a power spectrum candidate. We then discuss the selection of our final candidate list and the application of our final verification procedures. In § 3.2, we describe how the source strength and waveform affect spectral power. This information is used in § 3.3 to place limits on the pulsed fraction and duty cycle for each source. In § 3.4, we describe our best candidate and how it was debunked.

3.1. Significance

In the absence of a signal, the power P in a given spectral bin follows a χ^2 distribution. More precisely, since our individual spectra were normalized to a mean value of 1, $2P$ is χ^2 distributed with 2 degrees of freedom. If P_m is a sum of powers from m independent frequency bins, then $2P_m$ is χ^2 distributed with $2m$ degrees of freedom. The probability p that a power sum P_m will exceed some given threshold P_0 is

$$p(P_m > P_0) = e^{-P_0} \sum_{j=0}^{m-1} \frac{P_0^j}{j!} . \qquad (16)$$

Our searches of four-harmonic power sums provided our best sensitivity, and we consider only four-harmonic candidates from now on.

The above probability applies to an individual statistical trial. To determine the significance of a candidate, we must account for all the trials in the search—all the fundamental frequencies (up to 40 Hz) in all of the power spectra (one for each $\dot{f}$ trial) for all of the EGRET sources searched. Corresponding to each fundamental frequency bin, there are nine different four-harmonic sums, and after the local oversampling analysis, we include two additional factors of 8, accounting for the increases in frequency and frequency-derivative resolution. Thus, by the final verification stage, we had effectively searched

$$N_{\text{trials}} \approx 4 \times 10^{14} \text{ (Crab-like search space)} \qquad (17)$$

four-harmonic trials. For the magnetar search, we had

$$N_{\text{trials}} \approx 5 \times 10^{11} \text{ (magnetar search space)} . \qquad (18)$$

Note that these four-harmonic sums were not all truly statistically independent, so we are overestimating N_{trials}.

The significance of a candidate with power P_0 (i.e., the probability that its power was produced by noise) is, therefore,

$$S \approx 1 - [1 - p(P_m > P_0)]^{N_{\text{trials}}} \approx N_{\text{trials}} p(P_m > P_0) , \qquad (19)$$

where the last approximation holds for large P_0. For the Crab-like searches, $m = 4$, while for the magnetar searches, $m = 4\mathscr{S} = 16$.

Unfortunately, even our best search candidates had a significance of $S \sim 1$. All four-harmonic, 4 bin (Crab search) candidates with $P_0 \geq 36$ were subjected to further testing. These "candidates" were not at all statistically significant; rather, they represented only the expected tail of the noise power distribution. Sixty-four independent $(f, \dot{f})$ candidates met this criterion. Most appeared in the candidate list several times, with various nearby values of f or $\dot{f}$, for a total of 582 final candidates. For each candidate, we calculated the power in the next four harmonics and analyzed the pulse profile. One candidate stood out after these analyses, and we describe it in some detail below (§ 3.4). All the candidates were then reanalyzed using PSF-weighted data, and in all cases the powers dropped, which is unequivocally fatal. For the magnetar search, the cutoff power was $P_0 = 53$ (again, corresponding to the highest expected noise powers, $S \sim 1$), resulting in a total of 224 candidates (56 independent), all of which were similarly eliminated.

3.2. Relating Spectral Power to Source Properties

For a given point source, the selected data set contains a total of N_t photons, N_s of which were emitted by the source. We assume that the source has some DC component and that only a fraction $\mathscr{F}$ of these source photons actually contribute to the pulsation. Using the arrival times of these photons, we calculate a power spectrum and normalize it as described above. The expected spectral power in a single harmonic is

$$\langle P \rangle \approx 1 + \alpha \mathscr{F}^2 \frac{N_s^2}{N_t} \qquad (20)$$

(Buccheri, Sacco, & Ozel 1987). The parameter α ranges from 0 to 1 as the waveform's duty cycle decreases from 100% (no pulsation) to 0% (δ-function). For a sinusoidal signal, $\alpha = \frac{1}{4}$ (see, e.g., van der Klis 1989). If we sum the powers from h harmonics, we expect

$$\langle P_h \rangle \approx h + \alpha_h \mathscr{F}^2 \frac{N_s^2}{N_t} . \qquad (21)$$

Note that for a sinusoid, $\alpha_h = \frac{1}{4}$ for all values of h since there is no signal power in higher harmonics. For a pure δ-function waveform, in which all the photons are emitted with the same phase, $\alpha_h = h$. In all cases, $0 \leq \alpha_h \leq h$.

The source strength N_s^2/N_t is estimated for each source a priori, and the minimum detectable power threshold is set by the specifics of the search (e.g., for our Crab search, we can say that none of the data sets contain a pulsar signal with a four-harmonic power exceeding $P_{\max} = 36$). We can therefore place constraints on the pulsed fraction and the duty cycle of any pulsar signal contained in the data (provided it lies within our search phase space).

3.3. Upper Limits

If we wish to place upper limits on the source parameters with better than 50% confidence, we cannot simply solve equation (21) for $\alpha \mathscr{F}^2$. The spectral power produced by a periodic source will vary depending on particular samplings of the TOAs. Conversely, a measured spectral power can conceivably result from a wide range of intrinsic source

parameters. We must allow for this intrinsic statistical variation when calculating high confidence limits on the source parameters. We must also consider the fact that our search covers only a discrete grid of frequencies and frequency derivatives and generally will not recover the total signal power available in a data set. For these reasons, we determined our upper limits using Monte Carlo simulations. We calculated these limits at a confidence level of 95%.

Rather than simply report upper limits on the somewhat arcane combination $\alpha \mathscr{F}^2$, we chose a fiducial value for each parameter to constrain the other. Although it was certainly possible for us to have detected pulsations with realistic gamma-ray pulsar waveforms, we are unable to place useful upper limits on such signals. For most of our sources, we can only rule out pulsations at the 95% confidence level for waveforms that would have been easier to detect. The upper limits we report for the pulsed fraction are for a waveform typical of radio pulsars. Specifically, we assumed a single narrow Gaussian peak, with FWHM equal to 2.87% of the pulse period. This is the median radio pulse width quoted in the Princeton catalog (Taylor et al. 1993). To limit the duty cycle, we assumed a pulsed fraction of $\mathscr{F} = 100\%$, and we report lower limits on the FWHM of a single-peaked Gaussian waveform. The Crab-like search results are shown in Table 1; the magnetar search results are in Table 3.

3.4. Best Candidate

The source 2EG J1835 + 5919 produced our best candidate. Its largest four-harmonic, 12 bin power (after the FFT stage) was 55.98, and its largest four-harmonic, 4 bin power (after the local oversampling stage) was 38.67, neither of which was particularly significant, although the candidate was strong enough to make our final list. In fact, it appeared in the list a total of 27 times, with frequencies in the range $f = [32.9675598, 32.9675602]$ Hz and frequency derivatives in the range $\dot{f} = [-1.3483 \times 10^{-10}, -1.3427 \times 10^{-10}]$ Hz s^{-1}.

It was the power in the next four harmonics that first distinguished this candidate. Its best entry yielded a fifth through eighth harmonic power of 19.86, which has a significance better than $S \sim 0.002$. (Here, we have treated all 582 final candidates as independent, which they are not, so this estimate of the significance is conservative.) The pulse profile, shown in Figure 3, also looked very promising. The signal not only has rich harmonic content, but as we can see from the profile, those harmonics have similar phases; i.e., they have conspired to produce a single narrow peak.
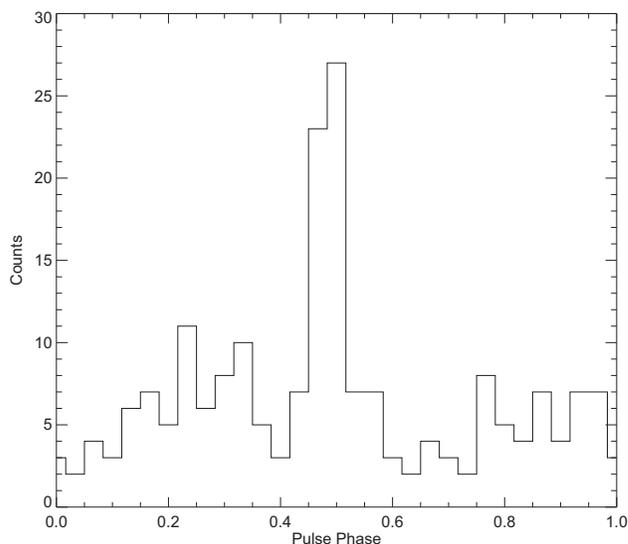

Fig. 3.—Pulse profile for our best candidate. The candidate is from 2EG J1835 + 5919, VP 212, with $f = 32.967560053$ Hz and $\dot{f} = -1.3463 \times 10^{-10}$ Hz s^{-1}. It was eliminated after PSF-weighting drastically degraded its significance.

We attempted a search for this signal in EGRET VPs 201–203 but did not find anything significant. This is not at all conclusive, however. As described above, even for a real pulsar, this verification method is not expected to have a high success rate. The final test was the most decisive. PSF-weighting the photons reduced the four-harmonic power from 38.67 to 24.01 (the power in the next four harmonics dropped from 19.86 down to 10.28), completely eliminating this as a pulsar candidate.

4. DISCUSSION

We knew from the start that our probability of detecting a new pulsar was not terribly high. With such a small number of known gamma-ray pulsars, however, even a single new identification would have been an important discovery. Unfortunately, our search detected no new gamma-ray pulsars, and we report here only upper limits.

At first glance, our upper limits on the pulsed fraction for each source (for the Crab-like search, see Table 1) ranging from 49% to 81% may not seem very stringent. Analysis of the Crab, Vela, and Geminga pulsars, however, reveals that all of these sources are essentially 100% pulsed in gamma rays. (It is noteworthy that the outer gap model of pulsar

TABLE 3

MAGNETAR SEARCH RESULTS

Source	N_s^2/N_t	$\dot{f}$ Trials	$\ddot{f}$ Trials	Total Trials	$\alpha \mathscr{F}^2$	Pulse FWHM[a] (%)	Pulsed Fraction[b] (%)
2EG J2020 + 4026	73	1161	6	6966	<0.75	>27	<44
2EG J0618 + 2234[c]	32	728	3	2184	<1.71	>15	<67
2EG J2019 + 3719[d]	34	1161	6	6966	<1.61	>16	<65
2EG J1835 + 5919	28	730	3	2190	<1.96	>13	<71
2EG J1021 − 5835[d]	27	708	3	2124	<2.03	>13	<73

[a] FWHM of a single Gaussian peak, expressed as a percentage of the pulse period; assumes 100% pulsed fraction.
[b] For typical radio pulsar waveform (see text).
[c] VP 1.0 only.
[d] The third EGRET catalog (Hartman et al. 1999) split 2EG J2019 + 3719 and 2EG J1021 − 5835 into multiple sources. The upper limits reported assume the validity of the second EGRET catalog (Thompson et al. 1995; see § 2.2.1).

gamma-ray emission also predicts a pulsed fraction of 100%.) It is therefore not unreasonable to expect most (if not all) of the photons from a source to contribute to any pulsation.

The waveform limits are a bit more troublesome. Our search was reasonably sensitive to signals with sharply peaked waveforms, such as those produced by typical radio pulsars. The pulse shapes of the known strong gamma-ray pulsars, however, exhibit dual narrow peaks, separated in phase by about $140°–180°$, with some emission (a "bridge") between the two peaks (Fierro 1996). The Geminga profile shown in Figure 2 is a good example. For our purposes, these waveforms can be characterized by the parameter α (see eq. [21]). By analyzing the power in the first four harmonics of the Crab, Vela, and Geminga pulsars, we determine $\alpha_C = 0.93$, $\alpha_V = 0.64$, and $\alpha_G = 0.41$, respectively. These values are to be compared with the "$\alpha \mathscr{F}^2$" column in Table 1, with $\mathscr{F} = 100\%$.

Thus, with very nearly 95% confidence, we would have detected a pulsar with a Crab-like waveform in 2EG J2020+4026 (100% pulsed). We cannot make such a strong statement about the Vela or Geminga waveforms, nor can we make any such claim for the weaker EGRET sources we searched. That is not to say that we had no chance of detecting pulsars with Vela-like or Geminga-like waveforms. We simply cannot claim with a high degree of confidence that we would have found them.

Direct timing of the EGRET data has not resulted in any new identifications. It now seems likely that further identifications of gamma-ray sources will come only from ongoing searches in other wavelengths and from future gamma-ray missions. In particular, the new generation of X-ray satellites (*CXO* and *XMM*) may resolve new counterparts to EGRET sources. Looking further ahead, the next-generation gamma-ray satellite *GLAST* promises to improve on EGRET's source localization and sensitivity by at least an order of magnitude. The improved source localization will make multiwavelength correlations easier and more reliable, while the increased effective area will greatly facilitate blind pulsar searches. McLaughlin & Cordes (2000) predict that 140 new gamma-ray pulsars will be detectable in blind searches with *GLAST* data, and the techniques described in this paper will be directly applicable to those searches.

REFERENCES

Baring, M. G., & Harding, A. K. 1997, in AIP Conf. Proc. 410, Fourth Compton Symposium, ed. C. D. Dermer, M. S. Strickman, & J. D. Kurfess (Woodbury: AIP), 638
———. 1998, ApJ, 507, L55
Bertsch, D. L., et al. 1992, Nature, 357, 306
Bhattacharya, D., Akyuz, A., Case, G., Dixon, D., & Zych, A. 1997, in AIP Conf. Proc. 410, Fourth Compton Symposium, ed. C. D. Dermer, M. S. Strickman, & J. D. Kurfess (Woodbury: AIP), 1137
Brady, P. R., & Creighton, T. 2000, Phys. Rev. D, 61, 082001
Brazier, K. T. S., Kanbach, G., Carraminana, A., Guichard, J., & Merck, M. 1996, MNRAS, 281, 1033
Brazier, K. T. S., Reimer, O., Kanbach, G., & Carraminana, A. 1998, MNRAS, 295, 819
Buccheri, R., Sacco, B., & Ozel, M. E. 1987, A&A, 175, 353
Esposito, J. A., et al. 1999, ApJS, 123, 203
Esposito, J. A., Hunter, S. D., Kanbach, G., & Sreekumar, P. 1996, ApJ, 461, 820
Fichtel, C. E., et al. 1994, ApJS, 94, 551
Fierro, J. M. 1996, Ph. D. thesis, Stanford Univ.
Fierro, J. M., et al. 1995, ApJ, 447, 807
———. 1993, ApJ, 413, L27
Halpern, J. P., & Holt, S. S. 1992, Nature, 357, 222
Hartman, R. C., et al. 1999, ApJS, 123, 79
Kaaret, P., & Cottam, J. 1996, ApJ, 462, L35
Kanbach, G., et al. 1994, A&A, 289, 855
———. 1989, in Proc. *Gamma Ray Observatory* Science Workshop, ed. W. N. Johnson (Vol. 2; Greenbelt: NASA), 1
Kaspi, V. M., Lackey, J. R., Mattox, J., Manchester, R. N., Bailes, M., & Pace, R. 2000, ApJ, 528, 445
Kouveliotou, C., et al. 1998, Nature, 393, 235
———. 1999, ApJ, 510, L115
Kuiper, L., Hermsen, W., Verbunt, F., Thompson, D. J., Stairs, I. H., Lyne, A. G., Strickman, M. S., & Cusumano, G. 2000, A&A, 359, 615

Lundgren, S. C., Zepka, A. F., & Cordes, J. M. 1995, ApJ, 453, 419
Malofeev, V. M., & Malov, O. I. 1997, Nature, 389, 697
Mattox, J. R., Koh, D. T., Lamb, R. C., Macomb, D. J., Prince, T. A., & Ray, P. S. 1996, A&AS, 120, C95
McLaughlin, M. A., & Cordes, J. M. 2000, ApJ, 538, 818
McLaughlin, M. A., Mattox, J. R., Cordes, J. M., & Thompson, D. J. 1996, ApJ, 473, 763
Melatos, A. 1999, ApJ, 519, L77
Nel, H. I., et al. 1996, ApJ, 465, 898
Nice, D. J., & Sayer, R. W. 1997, ApJ, 476, 261
Nolan, P. L., et al. 1993, ApJ, 409, 697
Ramanamurthy, P. V., et al. 1995, ApJ, 447, L109
Ramanamurthy, P. V., Fichtel, C. E., Kniffen, D. A., Sreekumar, P., & Thompson, D. J. 1996, ApJ, 458, 755
Roberts, M. S. E., & Romani, R. W. 1998, ApJ, 496, 827
Romani, R. W., & Yadigaroglu, I. A. 1995, ApJ, 438, 314
Shitov, Y. P. 1999, IAU Circ. 71102
Sturner, S. J., & Dermer, C. D. 1995, A&A, 293, L17
Sturner, S. J., Dermer, C. D., & Mattox, J. R. 1996, A&AS, 120, C445
Taylor, J. H., Manchester, R. N., & Lyne, A. G. 1993, ApJS, 88, 529
Thompson, C., & Duncan, R. C. 1995, MNRAS, 275, 255
———. 1996, ApJ, 473, 322
Thompson, D. J., et al. 1994, ApJ, 436, 229
———. 1992, Nature, 359, 615
———. 1996, ApJS, 107, 227
———. 1995, ApJS, 101, 259
———. 1993, ApJS, 86, 629
Van der Klis, M. 1989, in Timing Neutron Stars, ed. H. Ögelman & E. van den Heuvel (Dordrecht: Kluwer), 27
Wallace, P. M., Griffis, N. J., Bertsch, D. L., Hartman, R. C., Thompson, D. J., Kniffen, D. A., & Bloom, S. D. 2000, ApJ, 540, 184
Yadigaroglu, I. A., & Romani, R. W. 1997, ApJ, 476, 347